Order–disorder structure of the δ{1k} phase in the Fe–Zn system determined by scanning transmission electron microscopy

Okamoto, Norihiko L.; Yasuhara, Akira; Inui, Haruyuki

Order-Disorder Structure of the δ_{1k} Phase in the Fe–Zn System Determined by Scanning Transmission Electron Microscopy

Norihiko L. Okamoto[1,2,*], Akira Yasuhara[3], and Haruyuki Inui[1,2]

[1]*Department of Materials Science and Engineering, Kyoto University, Kyoto 606-8501, Japan*

[2]*Center for Elements Strategy Initiative for Structure Materials (ESISM), Kyoto University, Kyoto 606-8501, Japan*

[3]*EM Application Group, JEOL Ltd., Akishima, Tokyo, 196-8558, Japan*

***Corresponding Author Contact Information:**

Norihiko L. Okamoto

Department of Materials Science and Engineering, Kyoto University

Sakyo-ku, Kyoto 606-8501, Japan

Tel: +81-75-753-5481

Fax: +81-75-753-5461

E-mail: okamoto.norihiko.7z@kyoto-u.ac.jp

Abstract

The crystal structure of the δ_{1k} phase in the Fe–Zn system has been investigated by scanning transmission electron microscopy. The δ_{1k} phase has a superlattice structure based on the δ_{1p} phase having a tripled periodicity along the *a*-axis direction of the δ_{1p} phase, accompanied by one-dimensional stacking disorder of structural blocks (called order-disorder packets) along the *c*-axis direction. The crystal structure can crystallographically be described in terms of the order–disorder (OD) theory so as to belong to the category IV OD structures composed of two types of non-polar OD layers (L_{2n} and M_{2n+1}). The tripled periodicity along the *a*-axis direction is due to chemical ordering of the constituent Fe and Zn atoms in the OD layer M_{2n+1}. Because of the tripled periodicity of the OD layer M_{2n+1}, three different equivalent stacking positions are generated in stacking an OD layer M_{2n+1} on top of the OD layer L_{2n}. Depending on the stacking order, the crystal structure of the δ_{1k} phase can be ordered with various periodicities along the stacking direction or completely disordered. Based on the OD theory, two maximum degree of order (MDO) polytypes belonging to the space groups of $P6_3/mcm$ (MDO1) and $R3c$ (MDO2) are deduced for the δ_{1k} phase. The most stable MDO polytype in the OD family of the δ_{1k} phase is determined experimentally to be the MDO2 polytype.

Keywords: Intermetallic compounds (IMCs); Scanning transmission electron microscopy (STEM); Electron diffraction; Single crystal; Superlattice

1. Introduction

Hot-dipped galvannealed (GA) steels have been widely used in the automobile industry because of their high corrosion resistance, weldability, and paintability [1]. GA steels are produced by immersing steel strips into a molten zinc bath followed by heat-treatment to alloy the zinc coating with the substrate iron through thermal diffusion. The coating layer usually consists of five intermetallic compounds, Γ (Fe_3Zn_{10}), Γ_1 ($Fe_{11}Zn_{40}$), δ_{1k} ($FeZn_7$), δ_{1p} ($Fe_{13}Zn_{126}$) and ζ ($FeZn_{13}$) phases [2-6], which appear in the zinc-rich domain of the Fe–Zn binary phase diagram. When GA steels are deformed under severe conditions such as press-forming operations, the coating layer occasionally fails by decohesion at the coating/substrate interface (flaking) or by intracoating cracking to form fine particles (powdering). Such coating failure is known empirically to be mitigated when the coating layer consists largely of the δ_1 (δ_{1k}/δ_{1p}) phase [7]. The δ_1 (δ_{1k}/δ_{1p}) phase has thus long been considered to be relatively ductile, playing an important role in deformation of the coating in the forming process of GA steels. However, we have recently revealed from micropillar compression tests made for polycrystals that both of the δ_{1k} and δ_{1p} phases are extremely brittle, exhibiting no appreciable plastic strain prior to premature fracture [8]. Although thermodynamics and crystallography of the relevant phases in the Fe–Zn binary system have been intensively investigated for several decades [3-5, 9-25], the information about the crystal structure of the δ_{1k} and δ_{1p} phases is very much limited. It is only relatively recently

that the crystal structure of the δ_{1p} phase has been refined by X-ray diffraction [22], while the crystal structure of the δ_{1k} phase has yet to be refined until now. Hong et al. [20] have reported that the δ_{1k} phase has a superlattice structure based on the δ_{1p} phase with the *a*-axis dimension three times that of the δ_{1p} phase, since they observed additional streaks in selected-area electron diffraction (SAED) patterns of the δ_{1k} phase at the corresponding positions. However, they neither explained the origin of the additional streaks (instead of diffraction spots) nor made any further structure refinement for the δ_{1k} phase [20]. The existence of structural disorder, which can easily be inferred from diffraction streaks, is considered to have prevented detailed structural analyses of the δ_{1k} phase by X-ray diffraction. Very recently, we have refined the crystal structure of the δ_{1p} phase by synchrotron X-ray diffraction combined with scanning transmission electron microscopy (STEM) [25], elucidating that the δ_{1p} phase comprises coordination polyhedra including Fe-centered normal and disordered Zn_{12} icosahedra[1], and Zn-centered Zn_{12} icosahedra and Zn_{16} icosioctahedra (as described in detail in the next section) but that Zn_{12} bicapped pentagonal prisms are not included unlike in the model of Belin et al.'s [22]. We have planned to refine the crystal structure of the δ_{1k} phase similarly by synchrotron X-ray diffraction combined with STEM.

In the present study, we make STEM investigation on the structure of the δ_{1k} phase at an ultra-high spatial resolution (~0.08 nm) to elucidate structural relationships between the δ_{1k}

[1]In disordered Zn_{12} icosahedra, positional disorder exists at the vertex sites with the occupancy of ⅓.

and δ_{1p} phases, paying special attention to the origin of additional streaks in SAED patterns. The results of crystal structure refinement by synchrotron X-ray diffraction will be published elsewhere [26].

2. Crystal structure of the δ_{1p} phase

The crystal structure of the δ_{1p} phase [25] is described here, since the crystal structure of the δ_{1k} phase is considered to be a superlattice structure based on the δ_{1p} phase. The δ_{1p} phase contains 556 atoms in a large hexagonal unit cell ($a^{(p)}$ = 1.28297 nm, $c^{(p)}$ = 5.72860 nm) with the space group of $P6_3/mmc$. The structure can be best described by considering the packing of coordination polyhedra including Fe-centered normal and disordered Zn_{12} icosahedra, and Zn-centered Zn_{12} icosahedra and Zn_{16} icosioctahedra (Fig. 1(a)). Fe-centered normal icosahedra are linked with one another so as to form two types of slabs (slabs S_A and S_B) parallel to the *c*-plane (Fig. 1(a)). These two types of slabs are stacked alternately along the *c*-axis, being bridged with each other by face-sharing with icosioctahedra. In addition, some Zn atoms that do not constitute any polyhedra (called dangling Zn atoms hereafter) appear between the alternately stacked slabs of Fe-centered normal icosahedra.

There exist two mirror planes at z = ¼ and ¾ and an inversion center at the origin, indicating that the lower and upper halves of the crystal structure of the δ_{1p} phase are crystallographically identical with each other but are related with each other by a

180°-rotation about the *c*-axis [25]. The crystal structure of the δ_{1p} phase is thus described to build up with structural blocks that are related with each other by a 180°-rotation about the *c*-axis and are alternately stacked on top of each other. These structural blocks having the thickness of $c^{(p)}/2$ are described in the present paper as P_{2n} $(0 \leq z \leq 1/2)$ and P'_{2n+1} $(1/2 \leq z \leq 1)$ (Figs. 1(a) and 4(a)).[2]

3. Experimental procedures

A solution growth method was employed to grow single crystals of the δ_{1k} phase. Elements (4N purity) with a molar ratio of Zn:Fe = 97.3:2.7 were sealed in a quartz ampoule under vacuum. The ampoule was heated in an electric muffle furnace at 1153 K for 24 h to completely mix the elements. Subsequently, the ampoule was quickly cooled down to 943 K, and then slowly to 903 K over 160 h (−0.25 K h^{-1}). Then, the ampoule was taken out from the furnace and broken to scoop up grown single crystals from the molten zinc, followed by air-cooling. We obtained large hexagonal prismatic crystals terminated by pyramidal faces with an approximate size of 10×10×25 mm^3. The chemical composition was measured on several crystals by energy dispersive X-ray spectroscopy (EDS) in a scanning electron microscope. The average composition was 13.0±0.4 at.%Fe. Slices parallel to (0001), $(2\bar{1}\bar{1}0)$ and $(1\bar{1}00)$ low-index crystallographic planes with a thickness of 200 μm were cut from the

[2]The apostrophe means that the structural block has the opposite orientation within the basal plane.

single crystals for transmission electron microscopy (TEM) observations. Subsequently, the slices were mechanically ground and polished until the thickness reaches ~40 μm, followed by perforation by ion milling with 3 keV Ar ions at 110 K. SAED patterns were taken with a JEM-2000FX TEM operated at 200 kV. Ultra-high-resolution (spatial resolution: ~0.08 nm) STEM imaging was made with a spherical-aberration-corrected JEOL JEM-ARM200F STEM operated at 200 kV. The probe convergence angle and the inner/outer detector angles for high-angle annular dark-field (HAADF) imaging were 22 and 90/370 mrad, respectively.

4. Results

4.1. Electron diffraction

Figs. 2(a)-(c) and (d)-(f) illustrate SEAD patterns of the δ_{1p} and δ_{1k} phases taken along the [0001], $[1\bar{1}00]$, and $[2\bar{1}\,\bar{1}0]$ directions, respectively. In the SEAD pattern of the δ_{1k} phase with the [0001] incidence, additional diffraction spots are observed in all three equivalent rows of $hh\overline{2h}0$ systematic reflections at positions that divide the distance between the 0000 and $2\bar{1}\,\bar{1}0$ spots by three, as indicated by circles in Fig. 2(d). However, these additional diffraction spots observed in the SAED pattern of the [0001] incidence are turned out to be streaks in the $m/3[11\bar{2}\,l]^*$ reciprocal lattice rows ($m \neq 3n$, where m and n are integers) when the SAED pattern of the δ_{1k} phase with the $[1\bar{1}00]$ incidence is inspected, as indicated by arrows in Fig. 2(e). No streaks are observed in the corresponding positions in the SAED

pattern of the δ_{1p} phase with the $[1\bar{1}00]$ incidence (Fig. 2(b)). On the other hand, the SAED patterns of the δ_{1p} and δ_{1k} phases taken along the $[2\bar{1}\bar{1}0]$ direction are virtually identical with each other (Figs. 2(c) and (f)). These observations are basically identical with those reported by Hong et al. [20], who concluded that the δ_{1k} phase has a superlattice structure based on the δ_{1p} phase with the tripled *a*-axis dimension.

It should be noted here, however, that in the SAED pattern of the δ_{1k} phase with the $[1\bar{1}00]$ incidence, streaks are observed in the $m/3[11\bar{2}l]^*$ reciprocal lattice rows but not in the $n[11\bar{2}l]^*$ reciprocal lattice rows, indicating that streaks are not due to the occurrence of simple stacking faults. This is one of typical diffraction characteristics of the subject with one-dimensional disorder, in which the stacking order of structural blocks (representing the composition of the crystal itself) is virtually disordered [27-32].

4.2. STEM observation

HAADF-STEM images of the δ_{1p} and δ_{1k} phases taken along the $[1\bar{1}00]$ direction are shown in Figs. 3(a) and 3(b), respectively. The unit cell of the δ_{1p} phase is outlined by a solid frame in the figures. In accordance with the conclusion from SAED inspection that the δ_{1k} phase has a superlattice structure based on the δ_{1p} phase, there is no significant difference in the positions of bright spots in the HAADF-STEM images of the δ_{1p} and δ_{1k} phases. However, there is a noticeable difference in their intensity in the HAADF-STEM images for the two

phases. When the intensity profile is inspected along the [11 $\bar{2}$ 0] direction, a rather continuous fringe in the *c*-axis direction occurs every half the *a*-axis dimension ($a^{(p)}/2$ = ~0.64 nm) in the HAADF-STEM image of the δ_{1p} phase (Fig. 3(a)), whereas in the HAADF-STEM image of the δ_{1k} phase, every third fringe exhibits a stronger intensity (indicated by double arrows in Fig. 3(b)), making the periodicity along the [11 $\bar{2}$ 0] direction tripled ($3a^{(p)}/2$ = ~1.92 nm) when compared to the δ_{1p} phase. The tripled periodicity of the HAADF-STEM image for the δ_{1k} phase can clearly be seen in the intensity profile along the dashed line X−Y of Fig. 3(b), as shown in the bottom of Fig. 3(b). This is again in accordance with the observation of streaks in the *m*/3[11 $\bar{2}$ *l*]* reciprocal lattice rows in the SAED pattern of the [1$\bar{1}$00] incidence (Fig. 2(e)). This indicates that as outlined by dashed frames in Fig. 3(b), the structural block describing the crystal structure of the δ_{1k} phase has the tripled periodicity along the [11 $\bar{2}$ 0] direction with the same height (half the *c*-axis constant of the δ_{1p} phase ($c^{(p)}/2$ = ~2.86 nm)) as compared to the structural block for the δ_{1p} phase.

Since the intensity of atomic columns in the atomic-resolution HAADF-STEM image is approximately proportional to the square of the average atomic number [33], chemical ordering of the constituent Fe and Zn atoms must be responsible for the tripled periodicity of the structural block of the δ_{1k} phase along the [11 $\bar{2}$ 0] direction. Closer look at the structural blocks for the δ_{1k} phase (Fig. 3(d)) indicates that the intensity of some bright spots increases (indicated by solid circles in Fig. 3(d)) while that of others decreases (indicated by dashed

circles in Fig. 3(d)), when compared to the corresponding bright spots in the structural block for the δ_{1p} phase (Fig. 3(c)), so as to form the tripled periodicity along the [11$\bar{2}$0] direction. Possible reasons for the tripled periodicity include:

(i) The brighter atomic columns indicated by solid circles (blue/white/yellow) are occupied mainly by heavier Zn atoms,

(ii) The darker atomic columns indicated by dashed circles are occupied mainly by lighter Fe atoms,

(iii) Vacancies, if exist, are located in the darker atomic columns.

Unfortunately, the detailed information about the atomic coordinates for Fe and Zn atoms in the δ_{1k} phase cannot be extracted only from the STEM observations. Single-crystal X-ray diffraction analysis is underway in our research group [26] for a particular polytype of the δ_{1k} phase, which will be described later in Section 5.2.

Of significance to note in Fig. 3(b) is the loss of the regularity in the stacking of structural blocks with the triples periodicity along the [11$\bar{2}$0] direction. This can be inspected by checking the positions of every third strong fringes in the *c*-axis direction (double arrowed). In some cases, a structural block is stacked immediately above the lower one, but in other cases, a relative shift by either $\pm a^{(p)}/2$ along the *a*-axis direction occurs on their stacking. This indicates that there are three different stacking vectors to express the stacking of structural blocks for the δ_{1k} phase with the tripled periodicity, as schematically illustrated in Figs.

4(b-d). These can be described as follows: a structural block is stacked

(i) immediately above (Fig. 4(b): A→A')

(ii) diagonally to the upper left of (Fig. 4(c): A→B')

(iii) diagonally to the upper right of (Fig. 4(d): A→C')

the lower structural block. As in the case of the δ_{1p} phase, adjacent two structural blocks are related with each other by a 180°-rotation about the *c*-axis. The loss of the regularity in the stacking of structural blocks is evident in Fig. 3(b), as their stacking order A-A'-B-A'-C- indicates. The crystal structure of the δ_{1k} phase thus should be described with the concept of order–disorder (OD) theory, in which a crystal structure is described with the symmetry of OD layers (three-dimensional objects with two-dimensional periodicity) and the relative relation between two adjacent OD layers [27-32].

5. Discussion

5.1. Crystal structure description with the OD theory

The concept of OD structures was first introduced by Dornberger-Schiff [27] and further developed by Dornberger-Schiff and her co-workers [28-30, 34], leading to the generalization of the basic concept of 'crystal' in a broad sense [32]. A crystal in a broad sense includes those with periodicity in two dimensions and non-periodicity in the third dimension and can be described in terms of three-dimensional objects with two-dimensional periodicity (OD

layers) stacked according to a specific law known as the vicinity condition that states every pair of two adjacent OD layers is symmetrically equivalent [32]. The OD layers are related by partial operations (POs). The POs converting an OD layer into itself are called λ-POs while those converting an OD layer into an adjacent one are called σ-POs. The set of λ-POs for a given OD layer constitutes one of the 80 layer groups [27, 28, 35]. The POs sustaining the orientation of the layer are denoted as τ-POs, while those turning the layer upside down are called ρ-POs. Both λ- and σ- POs can be either τ or ρ.

Although the δ_{1p} phase does not possess a non-periodic OD structure but does possess a fully ordered structure belonging to the space group of $P6_3/mmc$ [25], we will describe its crystal structure according to the OD theory (Section 5.1.1). Based on that description, the crystal structure of the δ_{1k} phase will be described subsequently according to the OD theory (Section 5.1.2).

5.1.1. The δ_{1p} phase

As illustrated in Figs. 1 and 4(a), the crystal structure of the δ_{1p} phase builds up with structural blocks with the thickness of $c^{(p)}/2$ stacked along the *c*-axis. However, the structural block is not the unique OD layer with which the structure is described according the OD theory. In fact, the structural block can be divided into two different OD layers denoted in the following as L_{2n} and M_{2n+1}:

(i) OD layer L_{2n}, comprising Fe-centered normal Zn_{12} icosahedra (slab S_A), as shown in Figs. 5(a) and (b). The layer group of the OD layer L_{2n} is $p\bar{3}m1$ (short symbol) or $Pmmm(\bar{3})111$ (full seven-entry symbol[3]). The origin of the layer is set at $\bar{3}m$ ($(x, y, z) = (0, 0, 0)$)[4]. The layer is non-polar. There is one λ-ρ plane at $z = 0$.

(ii) OD layer M_{2n+1}, comprising Fe-centered normal Zn_{12} icosahedra (slab S_B), Fe-centered disordered Zn_{12} icosahedra, Zn-centered Zn_{12} icosahedra and Zn_{16} icosioctahedra, and dangling Zn atoms, as shown in Figs. 5(c) and (d). The layer group of the OD layer M_{2n+1} is $p\bar{6}m2$ (short symbol) or $Pmmm(\bar{6})222$ (full seven-entry symbol). The origin of the layer is set at $\bar{6}m2$ ($(x, y, z) = (0, 0, 1/4)$. The layer is non-polar. There is one λ-ρ plane at $z = 1/4$.

Thus, the δ_{1p} phase can be considered to consist of these two OD layers stacked alternately along the $c^{(p)}$ direction. The diagrams of symmetry elements for the $p\bar{3}m1$ and $p\bar{6}m2$ layer groups corresponding to the λ-POs in the OD layers L_{2n} and M_{2n+1} are illustrated in Figs. 5(e) and (f), respectively [35]. Because the crystal structure is composed of two OD layers both of which are non-polar (as is evident from the presence of λ-ρ plane), the δ_{1p} phase can be considered to belong to the category IV OD structures [31, 37-39]. The choice of OD layers

[3] The OD notation for the layer groups follows the international notation, using Hermann–Mauguin symbols, in which the direction of missing periodicity is explicitly indicated by parentheses [28,31,34,36]. For trigonal/hexagonal lattices, the operations corresponding to all important directions $\boldsymbol{a}_1$, $\boldsymbol{a}_2$, $\boldsymbol{a}_3$, $\boldsymbol{c}$, $\boldsymbol{a}_2 - \boldsymbol{a}_3$, $\boldsymbol{a}_3 - \boldsymbol{a}_1$, and $\boldsymbol{a}_1 - \boldsymbol{a}_2$ (in the given order) have to be specified [27,34].

[4] Fractional coordinates are referred to the unit cell of the δ_{1p} phase.

in OD structures of category IV is not unique and a boundary between two adjacent OD layers can be set in more than one way [31]. For instance, dangling Zn atoms can be appended either to L_{2n} or to M_{2n+1} layers. The choice of the OD layers described above is thus one of several possible ones.

The so-called *NFZ* relation [29, 31, 32] is useful to consider the number of geometrically equivalent stacking positions of the OD layers. The *NFZ* relation calculates the value of *Z*, the number of the possible distinct positions of the OD layer L_{p+1} relative to the fixed position of the OD layer L_p. The value of *Z* depends on the order *N*, the general multiplicity of the group of the λ-τ-POs valid for the single OD layer L_p, as well as on the order *F*, the general multiplicity of the group of the λ-τ-POs valid both for the single OD layer L_p and for the pair of the adjacent OD layers L_p and L_{p+1}. For OD structures in the category IV, the value of *Z* is calculated through the relation, $Z = N/F$. In the case of the δ_{1p} phase, the order *N* for the OD layer L_{2n} is six out of 12 symmetry operations of the $p\bar{3}m1$ layer group [35]. Since all the six operations are valid for the pair of the adjacent OD layers L_{2n} and M_{2n+1}, the order *F* is also six. Thus, the number $Z = N/F = 6/6 = 1$, indicating that these is only one possible position for the OD layer M_{2n+1} to stack on top of the OD layer L_{2n}. This is a natural consequence of the fact that the δ_{1p} phase possesses a fully ordered structure belonging to the space group of $P6_3/mmc$ [25].

5.1.2. The δ_{1k} phase

When judged from the contrast behavior of the HAADF-STEM image of Fig. 3(d), chemical ordering to form a superlattice structure of the δ_{1k} phase is observed to occur in the structural block region corresponding to the OD layer M_{2n+1} of the δ_{1p} phase but not in the region corresponding to the OD layer L_{2n} of the δ_{1p} phase (see Figs. 1(a), 5(a,c)). Because of the tripled periodicity along the *a*-axis direction, we have to consider maximal *k*-subgroups (klassengleich subgroups: IIa, IIb, IIc) of the layer group $p\bar{6}m2$ (the OD layer M_{2n+1} of the δ_{1p} phase) for the layer group of the corresponding OD layer in the δ_{1k} phase [35]. These maximal *k*-subgroups include the layer group $h\bar{6}m2$ with a triple cell ($3a^{(p)}\times 3a^{(p)}$) (Fig. 6(b)).[5] However, a hexagonal lattice is generally described by means of the smallest hexagonal primitive cell so that we should adopt the layer group $p\bar{6}2m$ with a primitive cell ($\sqrt{3}\,a^{(p)}\times\sqrt{3}\,a^{(p)}$) whose translation vectors (*a*-axes) are rotated in the basal plane by 30° with respect to those for $p\bar{6}m2$ and $h\bar{6}m2$ (Fig. 6(b)) [35]. Due to this rotation of the *a*-axes, <1 $\bar{1}$00> and <11 $\bar{2}$ 0> directions in the δ_{1p} phase correspond to the <11 $\bar{2}$ 0> and <1$\bar{1}$00> directions in the δ_{1k} phase, respectively. However, we describe <11 $\bar{2}$ 0> and <1$\bar{1}$00> directions in the δ_{1k} phase as <1$\bar{1}$00>$_p$ and <11 $\bar{2}$ 0>$_p$, respectively, in the present paper referring to the parent lattice of the δ_{1p} phase unless otherwise specifically stated. The general positions (12*h* sites) in the layer group $p\bar{6}2m$ are shown in Fig. 6(c) [35]. The general

[5] "*H*"or "*h*" indicates that the cell is triply primitive with reference to the common basic vectors. The *H* or *h* cell has 'centering' points at 0,0,0; 2/3,1/3,0; 1/3,2/3,0 [Ref. 40].

positions (12*j* sites) in the layer group $p\bar{6}m2$ are split into three different 12*h* sites in the layer group $p\bar{6}2m$ as shown in Fig. 6(d). The relationships of the general and special positions between the layer groups $p\bar{6}m2$ and $p\bar{6}2m$ are tabulated in Supplementary Table 1. Chemical ordering of the constituent Fe and Zn atoms among these split sites are attributed to the tripled periodicity. The OD layer M_{2n+1} in the δ_{1k} phase projected along the stacking direction (*c*-axis) is shown Fig. 5(g) (no chemical ordering is incorporated in the figure). The diagram of symmetry elements for the $p\bar{6}2m$ layer group corresponding to the λ-POs in the OD layer M_{2n+1} in the δ_{1k} phase is illustrated in Fig. 5(h). Since the OD layer L_{2n} is nothing to do with the tripled periodicity along the *a*-axis direction, the OD layer L_{2n} in the δ_{1k} phase is exactly identical with that the OD layer L_{2n} in the δ_{1p} phase. In the case of the δ_{1k} phase, the order *N* for the OD layer L_{2n} should be tripled because the area of the translational net for the OD layer L_{2n} ($a^{(p)}\times a^{(p)}$) is one third that for the OD layer M_{2n+1} ($\sqrt{3}\,a^{(p)}\times\sqrt{3}\,a^{(p)}$) [41]. Thus, the order *N* is 6×3 = 18. The order *F* is six because all the six λ-τ-POs valid for the single OD layer M_{2n+1} are valid also for the pair of the adjacent OD layers L_{2n} and M_{2n+1}. Thus, the number $Z = N/F = 18/6 = 3$, indicating that there are three possible positions for the OD layer M_{2n+1} to stack on top of the OD layer L_{2n}. This is consistent with what is observed by HAADF-STEM imaging (Fig. 3(b)) and what is explained in terms of stacking vectors in Section 4.2 (Fig. 4). This ambiguity in the stacking order for the OD layers produces the OD character of the δ_{1k} phase.

The symmetry of an OD structure is not described by a space group but by a groupoid, which is a set of λ- and σ-POs [27-32]. A whole family of derivative structures described with the same set of λ- and σ-POs is called an OD groupoid family and is generally described with the so-called OD-groupoid family symbol, which consists of two lines [27-32]. For the OD structures in the category IV composed of two different kinds of OD layers, the first line presents the λ-POs of the layer groups of the constituting OD layers, while the second line presents the positional relation between the adjacent OD layers, given in a square bracket by two components of the vector connecting the origins of the two adjacent layers projected into the layer plane [31, 32, 37-39]. The OD groupoid family symbol for the δ_{1k} phase is thus described as,

$$\begin{matrix} Pmmm(\bar{3})11 & P222(\bar{6})mmm \\ [1/3,\ 2/3] & \end{matrix} \qquad (1)$$

It is sometimes more instructive and useful to describe OD structures with a structural unit larger than individual OD layers [42]. This structural unit is called an OD packet, which by definition is the smallest continuous part of the OD structure and represents the composition of the crystal itself [42]. The OD packet of the δ_{1k} phase consists of the two OD layers L_{2n} and M_{2n+1} with the packet boundaries coinciding with the λ-ρ plane of the OD layer L_{2n} (Fig. 1(a)). The OD packet is thus virtually identical with the structural blocks, P_{2n} and P'_{2n+1}, used for explaining the δ_{1p} structure in Section 2, although the tripled periodicity along the $[11\bar{2}0]_p$ direction was not incorporated in the explanation. The symmetry of the

OD packet for the δ_{1k} phase is identical with the symmetry of the OD layer M_{2n+1}, $p\bar{6}2m$. It is useful to further describe the OD packet with a symbolic figure, which simply illustrates the symmetry of the OD packet [43]. The OD packet of the δ_{1k} phase projected along the stacking direction and symbolic figure for the OD packet are shown in Figs. 7(a) and (b), respectively. The symbolic figure has threefold symmetry about the stacking direction and mirror planes perpendicular to the $<11\bar{2}0>_p$ directions. The origin of the adjacent packet P'_{2n+1} may be shifted relative to that of the packet P_{2n} by any of the following stacking vectors,

$$\boldsymbol{t}_1 = \boldsymbol{c}_0 \tag{2a}$$

$$\boldsymbol{t}_2 = \frac{2}{3}\boldsymbol{a}_1^{(k)} + \frac{1}{3}\boldsymbol{a}_2^{(k)} + \boldsymbol{c}_0 \tag{2b}$$

$$\boldsymbol{t}_3 = \frac{1}{3}\boldsymbol{a}_1^{(k)} + \frac{2}{3}\boldsymbol{a}_2^{(k)} + \boldsymbol{c}_0 \tag{2c}$$

where $\boldsymbol{c}_0$ correponds to the unit vector of the OD packet along the stacking direction ($c^{(p)}/2$). The schematic illustrations of the stacking vectors viewed along directions perpendicular and parallel to the stacking direction are shown in Figs. 4(b)-(d) and 7(c)-(e), respectively. The stacking vector $\boldsymbol{t}_1$ does not change the position of the stacked packet; A⇒A', B⇒B', C⇒C'. On the other hand, both $\boldsymbol{t}_2$ and $\boldsymbol{t}_3$ change the positions like A⇒B', B⇒C', C⇒A', and A⇒C', B⇒A', C⇒B', respectively. An infinite number of polytypes of the δ_{1k} phase are thus obtained by a random occurrence of the stacking vectors $\boldsymbol{t}_i$ (i = 1, 2, 3) (Fig. 7(f)).

5.2. Polytypes with maximum degree of order (MDO) for the δ_{1k} phase

Any OD groupoid family theoretically contains an infinite number of periodic and non-periodic polytypes. Among the periodic polytypes, the simplest ones are called maximum degree of order (MDO) polytypes [29, 31, 34, 37, 38, 44, 45]. In MDO polytypes, not only pairs but also triples (and quadruples, … *n*-tuples) of consecutive layers (packets) are geometrically equivalent [32]. Each MDO polytype is characterized by a generating operation, whose continuous application gives rise to the MDO structure. In the present case of the OD groupoid family for the δ_{1k} phase, one generating operation is the σ-PO of $n_{0,2}$=c_2, indicated in Fig. 7(c). Continuous application of this operation (rotation by 180° and translation by the vector $\boldsymbol{t}_1$) yields a MDO polytype (MDO1) with the A-A'- stacking sequence (Fig. 8(a)). The unit cell of the MDO1 polytype belongs to the space group of $P6_3/mcm$ with a hexagonal unit cell of $\boldsymbol{a}_1^{(MDO1)} = \sqrt{3}\boldsymbol{a}_1^{(p)}$, $\boldsymbol{a}_2^{(MDO1)} = \sqrt{3}\boldsymbol{a}_2^{(p)}$ and $\boldsymbol{c}^{(\mathrm{MDO1})} = 2\boldsymbol{c}_0 = \boldsymbol{c}^{(\mathrm{p})}$ because the σ-PO of $n_{0,2}$=c_2 becomes a total operation, *c* glide plane, in the hexagonal cell. In the Ramsdell notation, the MDO1 polytype is designated 2*H*. Another generating operation is the σ-PO of a glide plane of $n_{1/3,2}$, indicated in Fig. 7(d). Continuous application of this operation (rotation by 180° and translation by the vector $\boldsymbol{t}_2$) results in another MDO polytype (MDO2) with the A-B'-C-A'-B-C'- stacking sequence (Fig. 8(b)). The MDO2 polytype belongs to the space group of $R3c$ with the rhombohedral unit cell of $\boldsymbol{a}_1^{(MDO2)} = \sqrt{3}\boldsymbol{a}_1^{(p)}$, $\boldsymbol{a}_2^{(MDO2)} = \sqrt{3}\boldsymbol{a}_2^{(p)}$, and $\boldsymbol{c}^{(\mathrm{MDO2})} = 6\boldsymbol{c}_0 = 3\boldsymbol{c}^{(\mathrm{p})}$ because the σ-PO of $n_{1/3,2}$

becomes a total operation $g(1/3, 2/3, 1/6)$ in the rhombohedral cell. In the Ramsdell notation, the MDO2 polytype is designated 6*R*. Likewise, continuous application of the σ-PO of a glide plane of $n_{-1/3,2}$ (rotation by 180° and translation by the vector $\boldsymbol{t}_3$) results in the stacking sequence of A-C'-B-A'-C-B'- (Fig. 7(e)). However, this MDO polytype (MDO2') is identical with the MDO2 polytype because the stacking sequence for MDO2' is exactly a reversal of that for MDO2.

5.3. Diffraction patterns of MDO polytypes

Diffraction patterns observed for OD structures are usually composed of two different types of reflections; family reflections and characteristic reflections [31, 36]. Family reflections appear at the same positions for all polytypes as far as they belong to the same OD family, while characteristic reflections appear at different positions specific to a given polytype. Therefore, if some different polytypes are incorporated or if some stacking disorder is present, diffraction streaks are observed in the reciprocal lattice rows of characteristic reflections while discrete diffraction spots are preserved for family reflections, as far as the stacking order is only those allowed for the same OD family [32, 46]. This is exactly what is observed in the SAED patterns of Figs. 2(d)-(f) for the δ_{1k} phase. The reflection conditions for the family reflections can be obtained by considering reflection conditions for the so-called 'family structure', a fictitious superimposed structure that is obtained by

simultaneous application of all possible σ-POs [31, 32, 46]. The reflection conditions for the family reflections of the δ_{1k} phase are described as follows:

$$\begin{aligned} &H\bar{H}0L : L = 2n \ (n : \text{integer}) \\ &000L : L = 2n \ (n : \text{integer}) \end{aligned} \tag{3}$$

where the indices in capital letters refer to the unit cell of the MDO1 (2*H*) polytype. The SAED patterns of the family structure with the $[1\bar{1}00]_p$ and $[2\bar{1}\bar{1}0]_p$ incidences calculated with the above reflection conditions are illustrated respectively in Figs. 9(b) and (g). Figs. 9(a) and (f) are the corresponding portions of the experimental SAED patterns reproduced from Figs. 2(e) and (f), respectively. The SAED patterns of the MDO1 (2*H*) and MDO2 (6*R*) polytypes, both of which are derived as the simplest OD structures in the present study, were calculated for the $[1\bar{1}00]_p$ and $[2\bar{1}\bar{1}0]_p$ incidences, as shown in Figs. 9(c-e), and (h,i), respectively. For the MDO2 (6*R*) polytype, the SAED patterns with the $[2\bar{1}\bar{1}0]_{MDO2}$ and $[\bar{2}110]_{MDO2}$ incidences (Figs. 9(d) and (e)) corresponding to that with the $[1\bar{1}00]_p$ were calculated, taking into account the rhombohedral symmetry. The calculated SAED patterns with the $[1\bar{1}00]_{MDO1}$ and $[1\bar{1}00]_{MDO2}$ incidences (Figs. 9(h) and (i)) are virtually both identical with the corresponding calculated SAED pattern for the family structure (Figs. 9(g)), since no characteristic reflections are contained. These two calculated SAED patterns of the MDO1 and MDO2 polytypes thus coincide with the corresponding experimental SAED pattern (Figs. 9(f)). In the three calculated SAED patterns of the MDO1 and MDO2 polytypes with the corresponding $[1\bar{1}00]_p$ incidence (Figs. 9(c)-(e)), on the other hand, characteristic reflections

are observed to appear at different specific positions depending on polytype in the $m[01\bar{1}L]^*$ reciprocal lattice rows ($m \neq 3n$, where m and n are integers) as indicated by double arrows, in addition to their common family reflections. The $[1\bar{1}00]_p$ SAED patterns calculated for the MDO1 and MDO2 polytypes (Figs. 9(c-e)) are overlaid and shown in Fig. 9(j). The characteristic reflections form dense reciprocal lattice rows along the $\boldsymbol{c}^*$ direction as indicated by double arrows. Diffraction streaks observed experimentally in the $m[01\bar{1}L]^*$ reciprocal lattice rows in Fig. 9(a) thus originate from the incorporation of some different polytypes of the same OD family accompanied by stacking disorder.

In order to explore the most stable MDO polytype of the OD family for the δ_{1k} phase, one of the single crystals grown by the solution growth method was annealed at 673 K for 9 days. A SAED pattern observed along the $[1\bar{1}00]_p$ direction for the annealed crystal is shown in Fig. 10(a). Streaks observed in the $m[01\bar{1}L]^*$ reciprocal lattice rows of the characteristic reflections before annealing (Figs. 1(c) and 9(a)) are no longer observed, and only discrete diffraction spots are observed in reciprocal lattice rows of both family and characteristic reflections. The positions of discrete diffraction spots in the reciprocal lattice rows of the characteristic reflections coincide with those calculated for the MDO2 polytypes (with the $[2\bar{1}\bar{1}0]_{MDO2}$ incidence) shown in Figs. 9(d) and 10(b). The HAADF-STEM image of the same annealed crystal taken along the $[2\bar{1}\bar{1}0]_{MDO2}$ direction (Fig. 10(c)) indicates that the stacking order of structural blocks is fairly regular and is the type of A-B'-C-A'-B-C'-, being

consistent with that for the MDO2 polytype, as described in Section 5.2. The MDO2 polytype is thus determined experimentally to be the most stable MDO polytype for the δ_{1k} phase. Crystal structure refinement for the δ_{1k} phase by X-ray diffraction is underway in our research group with the use of a single crystal of the MDO2 polytype [26]. The δ_{1k} phase existing in a thin coating layer of GA steels is usually far from the equilibrium state because of continuous diffusion of Fe from the substrate steel. Even after prolonged annealing, the δ_{1k} phase in the coating layer of GA steels cannot form in the most stable polytype (MDO2) but exhibit various OD structures, in which the stacking order for structural blocks is virtually disordered. This may be one of the reasons why crystal structure refinement for the δ_{1k} phase by X-ray diffraction has been difficult. In the present study, on the contrary, it has been realized that STEM is very powerful to determine the OD structures because it facilitates the direct observation of the stacking sequence of building layers whether it is regular or random.

6. Conclusions

(1) The δ_{1k} phase has a superlattice structure based on the δ_{1p} phase with a tripled periodicity along the $[11\bar{2}0]_p$ direction accompanied by one-dimensional stacking disorder of structural blocks along the *c*-axis direction. The crystal structure can thus be crystallographically described in terms of the order–disorder (OD) theory.

(2) The δ_{1k} phase belongs to the category IV OD structure composed of two types of

non-polar OD layers (L_{2n} and M_{2n+1}). The tripled periodicity along the $[11\bar{2}0]_p$ direction is attributed to chemical ordering occurring in the OD layer M_{2n+1}. Due to the tripled periodicity, there are three possible equivalent positions to stack an OD layer M_{2n+1} on top of an OD layer L_{2n}. The OD groupoid family symbol expressing the OD structures of the δ_{1k} phase is:

$$Pmmm\left(\bar{3}\right)11 \qquad P222\left(\bar{6}\right)mmm$$
$$[1/3,\ 2/3]$$

(3) The space groups for the two simplest forms (MDO polytypes) of the δ_{1k} phase are determined to be $P6_3/mcm$ (MDO1) and $R3c$ (MDO2). In the Ramsdell notation, these forms are designated 2*H* and 6*R*, respectively. The most stable MDO polytype in the OD family of the δ_{1k} phase is experimentally determined to be the MDO2 polytype (6*R*).

Acknowledgements

This work was supported by JSPS KAKENHI grant numbers 24246113 and 25709066, and the Elements Strategy Initiative for Structural Materials (ESISM) from the Ministry of Education, Culture, Sports, Science and Technology (MEXT) of Japan, and in part by Advanced Low Carbon Technology Research and Development Program (ALCA) from the Japan Science and Technology Agency (JST). This work was also supported by Research Promotion Grant from ISIJ and Grants for Technical Research from JFE 21st Century Foundation.

References

[1] Marder AR. Prog Mater Sci 2000;45:191.

[2] Kubaschewski O. Iron - Binary Phase Diagrams. Berlin: Springer-Verlage, 1982.

[3] Su XP, Tang NY, Toguri JM. J Alloys Compd 2001;325:129.

[4] Nakano J, Malakhov DV, Purdy GR. Calphad 2005;29:276.

[5] Kainuma R, Ishida K. Tetsu to Hagane 2005;91:349.

[6] Villars P. Pearson's Handbook: Crystallographic Data for Intermetallic Phases. Amsterdam: ASM International, 1997.

[7] Kato C, Koumura H, Uesugi Y, Mochizuki K. Influence of Phase Composition on Formability of Galvannealed Steel Sheet. In: Marder AR, editor. TMS Annual Meeting, The Physical Metallurgy of Zinc Coated Steel. San Francisco, CA: TMS, 1994. p.241.

[8] Okamoto NL, Kashioka D, Inomoto M, Inui H, Takebayashi H, Yamaguchi S. Scripta Mater 2013;69:307.

[9] Bablik H, Götzl F, Halla F. Z Metallkd 1938;8:249.

[10] Schramm J. Z Metallkd 1938;30:122.

[11] Ghoniem MA, Lohberg K. Metall 1972;26:1026.

[12] Bastin GF, Vanloo FJJ, Rieck GD. Z Metallkd 1974;65:656.

[13] Perrot P, Dauphin JY. Calphad 1988;12:33.

[14] Petersen S, Spencer PJ, Hack K. Thermochim Acta 1988;129:77.

[15] Reumont G, Perrot P, Fiorani JM, Hertz J. J Phase Equilib 2000;21:371.

[16] Johansson A, Ljung H, Westman S. Acta Chem Scand 1968;22:2743.

[17] Brandon JK, Brizard RY, Chieh PC, Mcmillan RK, Pearson WB. Acta Crystallogr B 1974;30:1412.

[18] Koster AS, Schoone JC. Acta Crystallogr B 1981;37:1905.

[19] Brown PJ. Acta Crystallogr 1962;15:608.

[20] Hong MH, Saka H. Scripta Mater 1997;36:1423.

[21] Uwakweh ONC, Liu ZT, Jordan A, Chakoumakos B, Spooner S, Maziasz P. Metall Mater Trans A 2000;31:2739.

[22] Belin CHE, Belin RCH. J Solid State Chem 2000;151:85.

[23] Belin R, Tillard M, Monconduit L. Acta Crystallogr C 2000;56:267.

[24] Okamoto NL, Inomoto M, Adachi H, Takebayashi H, Inui H. Acta Mater 2014;65:229.

[25] Okamoto NL, Tanaka K, Yasuhara A, Inui H. Acta Crystallogr B 2014;70:275.

[26] Okamoto NL, Inui H. to be submitted.

[27] Dornberger-Schiff K. Acta Crystallogr 1956;9:593.

[28] Dornberger-Schiff K. Acta Crystallogr 1959;12:173.

[29] Dornberger-Schiff, K. Abh Dtsch Akad Wiss 1964;3:1.

[30] Dornberger-Schiff K. Krist Techn 1979;14:1027.

[31] Ďurovič S. Fundamentals of the OD theory. In: Merlino S, editor. Modular Aspects of Minerals, vol. 1. Budapest, Hungary: Eőtvős University Press, 1997. p.3.

[32] Ferraris G, Makovicky E, Merlino S. Crystallography of Modular Materials. Oxford, UK: Oxford University Press, 2008.

[33] Pennycook SJ, Boatner LA. Nature 1988;336:565.

[34] Dornberger-Schiff K. Lehrgang über OD-Strukturen. Berlin: Akademie Verlag, 1966.

[35] Kopsky V, Litvin DB, editors. International Tables for Crystallography, Vol. E: Superperiodic group. Chichester, UK: John Wiley & Sons, Ltd, 2010.

[36] Durovic S, Hybler J. Z Kristallogr 2006;221:63.

[37] Dornbergerschiff K, Grell H. Acta Crystallogr A 1982;38:491.

[38] Grell H, Dornbergerschiff K. Acta Crystallogr A 1982;38:49.

[39] Merlino S, Orlandi P, Perchiazzi N, Basso R, Palenzona A. Can Mineral 1989;27:625.

[40] Hahn T. International Tables for Crystallography, Vol. A: Space-group symmetry. Dordrecht, The Netherlands: Springer, 2005.

[41] Dornberger-Schiff K, Durovic S. Clays Clay Miner 1975;23:219.

[42] Durovic S. Acta Crystallogr B 1974;30:76.

[43] Hybler J, Durovic S. Acta Crystallogr A 2009;65:501.

[44] Yokobayashi H, Kishida K, Inui H, Yamasaki M, Kawamura Y. Acta Mater 2011;59:7287.

[45] Kishida K, Yokobayashi H, Inui H, Yamasaki M, Kawamura Y. Intermetallics 2012;31:55.

[46] Merlino S. OD approach in ninerals: examples and applications. In: Merlino S, editor. Modular Aspects of Minerals, vol. 1. Budapest, Hungary: Eőtvős University Press, 1997. p.29.

Figure Legends

Fig. 1. (a) Crystal structure of the δ_{1p} phase projected along the $[2\bar{1}\,\bar{1}\,0]_p$ direction. The constituting OD layers and packets are described in the right-hand of the figure. (b) Schematic illustration of the 24*l* Wyckoff sites, the general positions in the space group of $P6_3/mmc$.

Fig. 2. SAED patterns taken along the (a,d) [0001], (b,e) $[1\bar{1}00]$, and (c,f) $[2\bar{1}\,\bar{1}\,0]$ directions for the (a-c) δ_{1p} and (d-f) δ_{1k} phases, respectively. Superlattice spots and streaks are indicated by circles and arrows in (d) and (e), respectively.

Fig. 3. HAADF-STEM images of the (a) δ_{1p} and (b) δ_{1k} phases taken along the $[1\bar{1}00]$ direction. The solid frame indicates the unit cell of the δ_{1p} phase. Single and double arrows in (b) indicate slightly darker and brighter atomic columns. The intensity profile along the dashed line X−Y is shown in the bottom of (b). (c,d) Magnified STEM-HAADF images of (a) and (b), respectively.

Fig. 4. Schematic illustrations of stacking manners of the structural blocks with the thickness of $c^{(p)}/2$ in the (a) δ_{1p} and (b-d) δ_{1k} phases, respectively. There are three different stacking manners in the δ_{1k} phase.

Fig. 5. (a,c) $[2\bar{1}\,\bar{1}\,0]$ and (b,d) [0001] projections of the OD layers (a,b) L_{2n} and (c,d) M_{2n+1}, respectively, in the δ_{1p} phase. (e,f) Diagrams of symmetry elements for the $p\bar{3}m1$ and $p\bar{6}m2$ layer groups corresponding to the λ-POs in the OD layers L_{2n} and M_{2n+1}, respectively. (g) [0001] projection of the OD layer M_{2n+1} in the δ_{1k} phase. (h) Diagram of symmetry elements for the $p\bar{6}2m$ layer group corresponding to the λ-POs in the OD layer M_{2n+1} in the δ_{1k} phase.

Fig. 6. (a) General positions in the layer group $p\bar{6}m2$ for the OD layer M_{2n+1} in the δ_{1p} phase. (b) Cell dimensions of triple and primitive cells with the layer groups of

$h\bar{6}m2$ $p\bar{6}2m$, respectively. (c) General positions in the layer group $p\bar{6}2m$ for the OD layer M_{2n+1} in the δ_{1k} phase. (d) Site splitting of the general positions 12*j* sites in the layer group $p\bar{6}m2$ into three different 12*h* sites in the layer group $p\bar{6}2m$.

Fig. 7. (a) [0001] projection of the OD packet in the δ_{1k} phase. (b) Arrays of symbolic figures showing the symmetry of the OD packet. (c-e) Three different manners of stacking the adjacent OD packet on the preceding OD packet at the position A. (c) A⇒A' with the stacking vector $\boldsymbol{t}_1$, (d) A⇒B' with the stacking vector $\boldsymbol{t}_2$, and (e) A⇒C' with the stacking vector $\boldsymbol{t}_3$. Symmetry elements of the σ-POs are shown in (d) and (e). (f) Schematic representation of the sequence of the stacking vectors for MDO polytypes and a non-periodic OD structure in the δ_{1k} phase.

Fig. 8. Stacking sequence of OD packets for the (a) MDO1 and (b) MDO2 polytypes.

Fig. 9. SAED patterns (a,f) experimentally observed, (b,g) calculated for the family structure, (c,h) calculated for the MDO1 polytype, and (d,e,i) calculated for the MDO2 polytype for the $[1\bar{1}00]_p$ and $[2\bar{1}\bar{1}0]_p$ incidences, respectively. The corresponding incidences for each of the MDO polytypes are shown in the top-right of the SAED patterns. (j) SAED patterns calculated for the MDO1 and MDO2 polytypes for the $[1\bar{1}00]_p$ incidence (c-e) are overlaid. Rows of the characteristic reflections are indicated by double arrows.

Fig. 10. (a) SAED pattern and (c) STEM-HAADF image of the annealed δ_{1k} single crystal taken along the $[1\bar{1}00]_p$ direction. (b) SAED pattern calculated for MDO2 polytype for the $[1\bar{1}00]_p$ incidence.

Figure1

Click here to download high resolution image

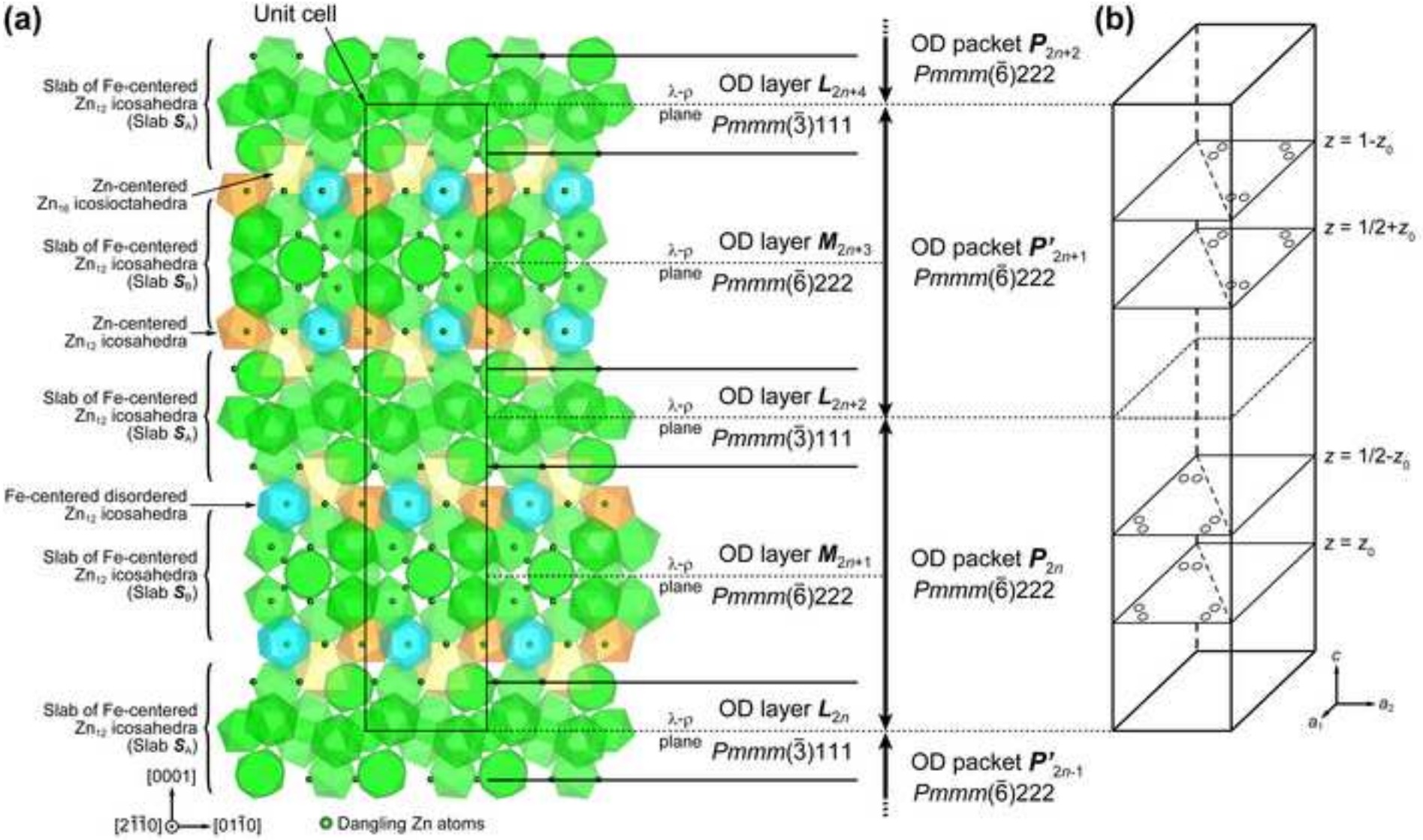

Figure2

Click here to download high resolution image

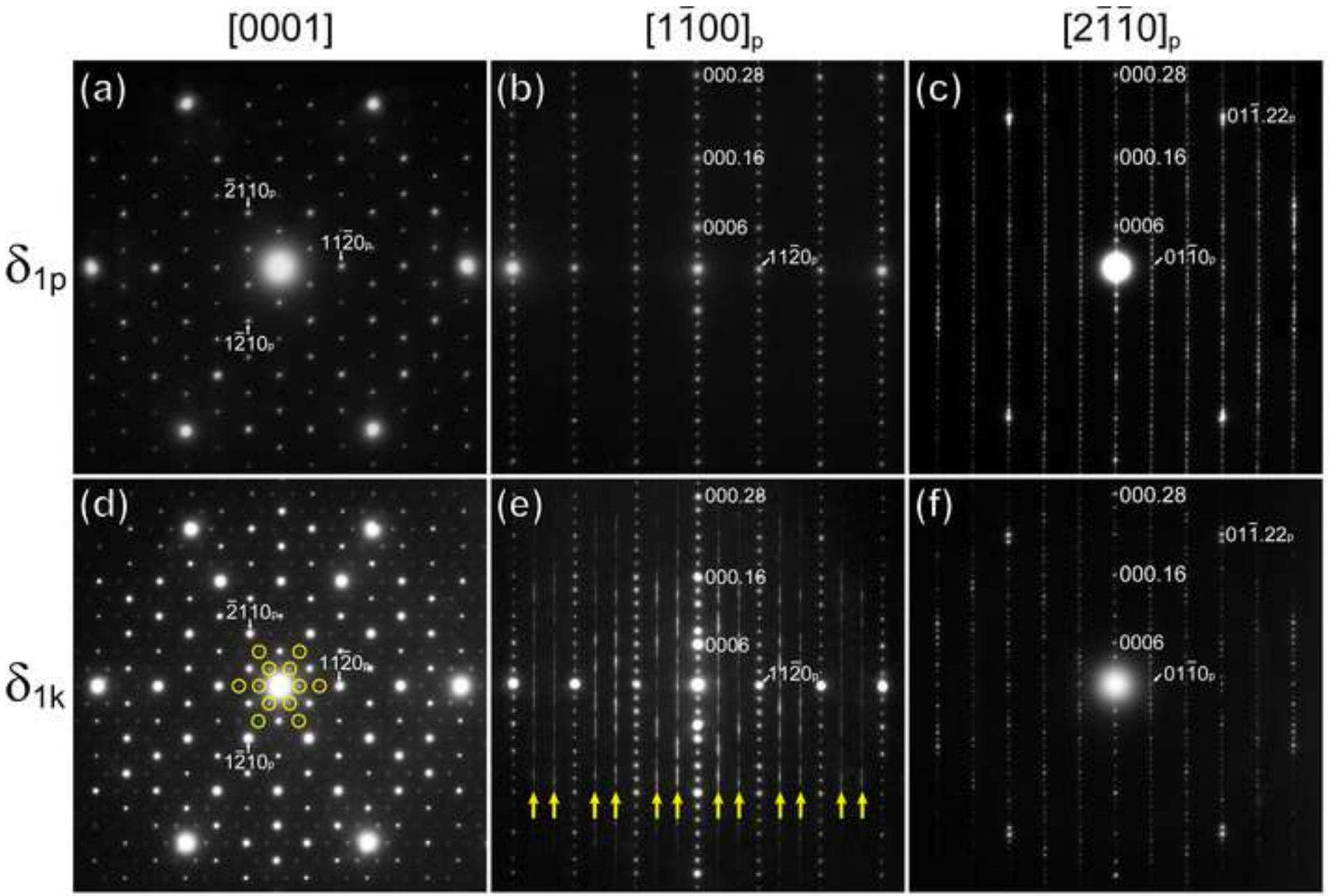

Figure3

Click here to download high resolution image

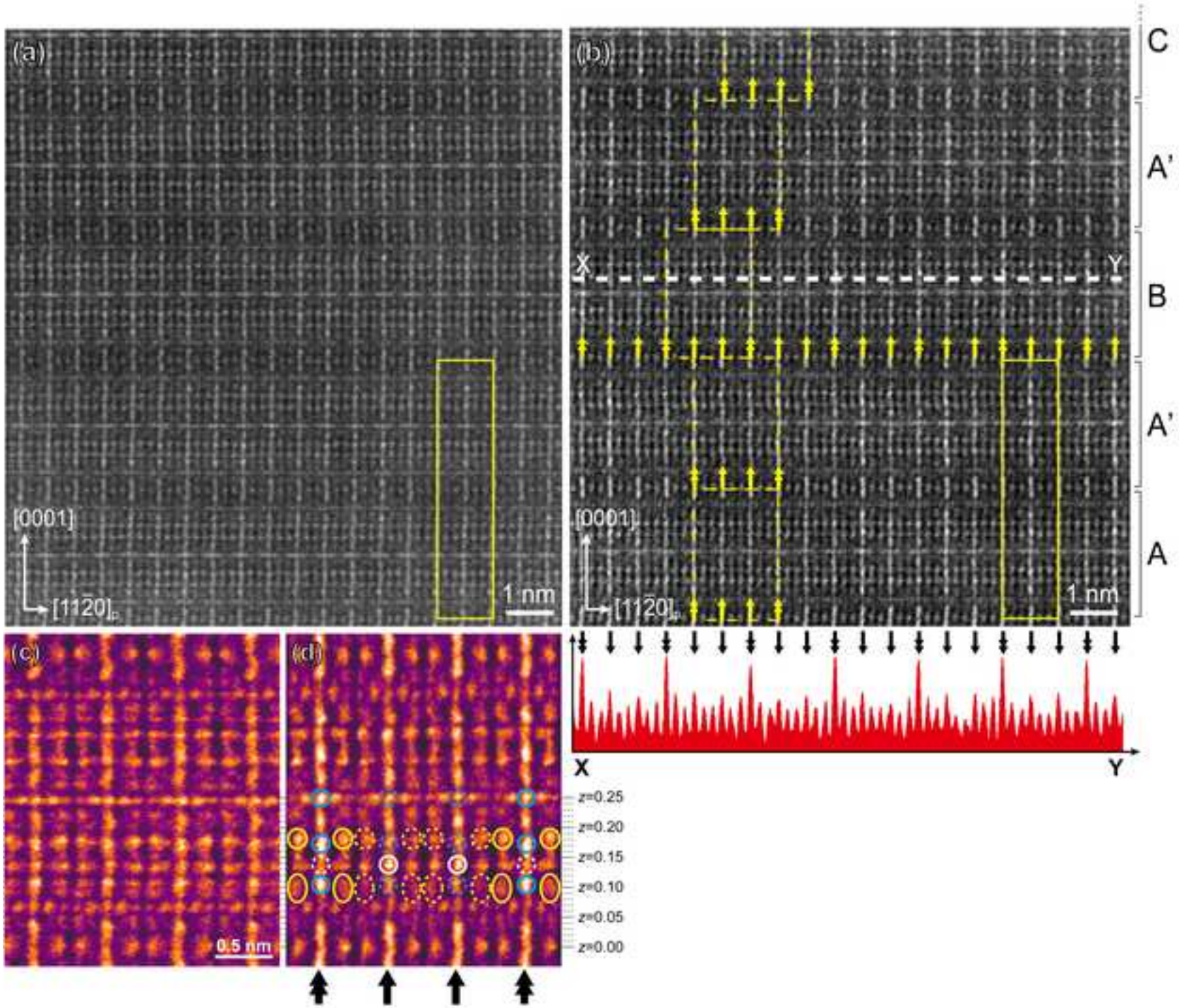

Figure4

Click here to download high resolution image

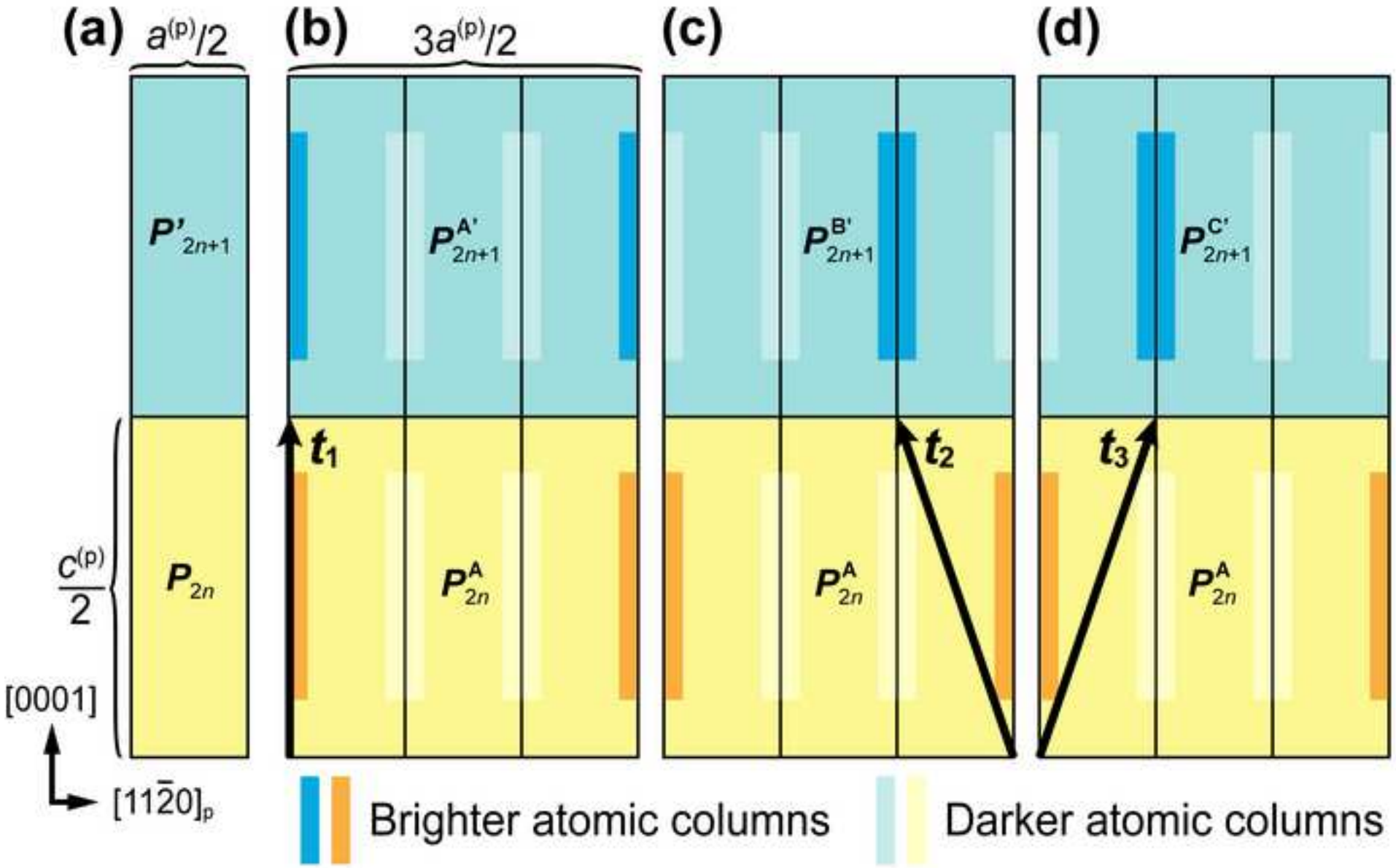

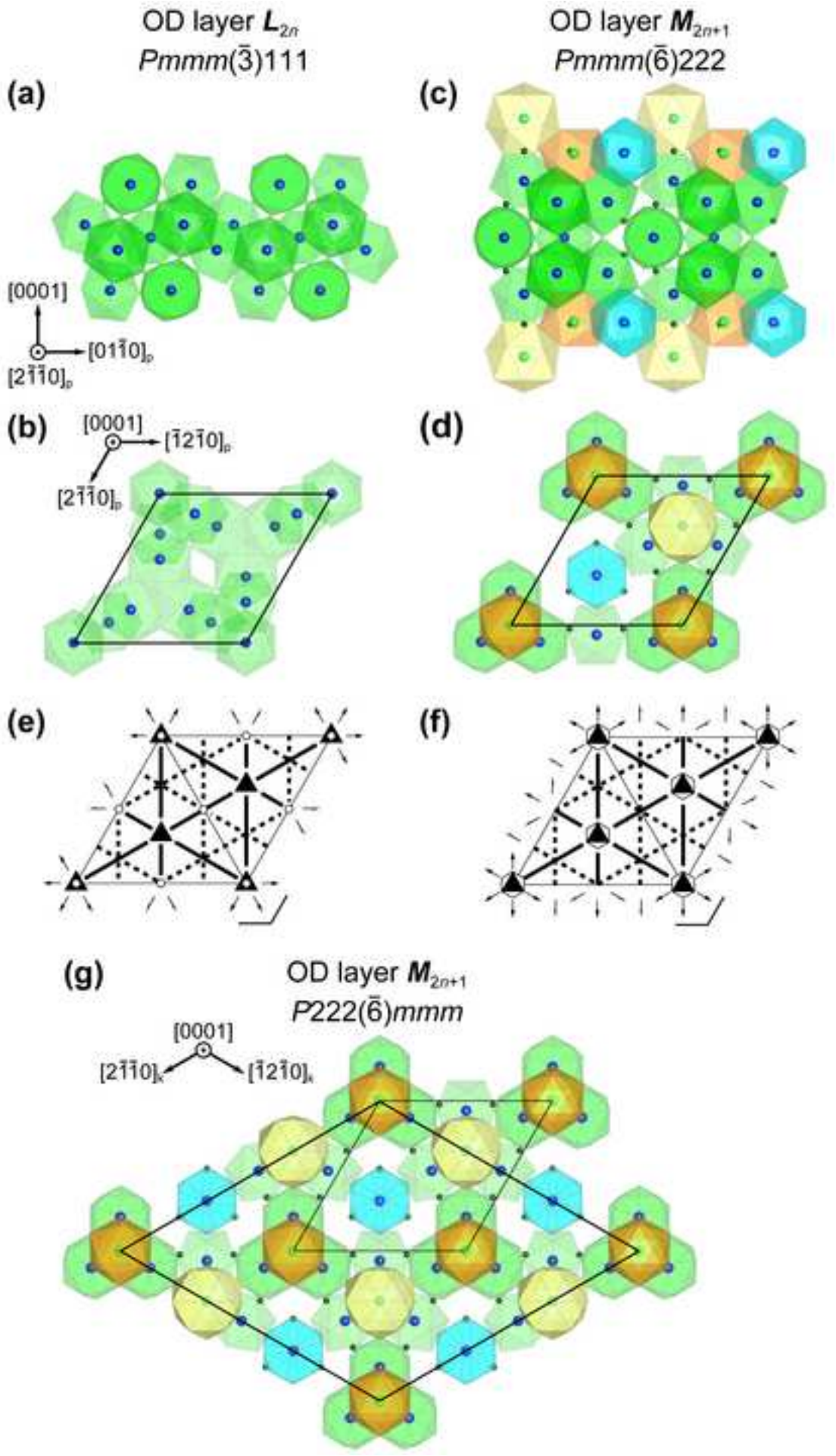

Figure6

Click here to download high resolution image

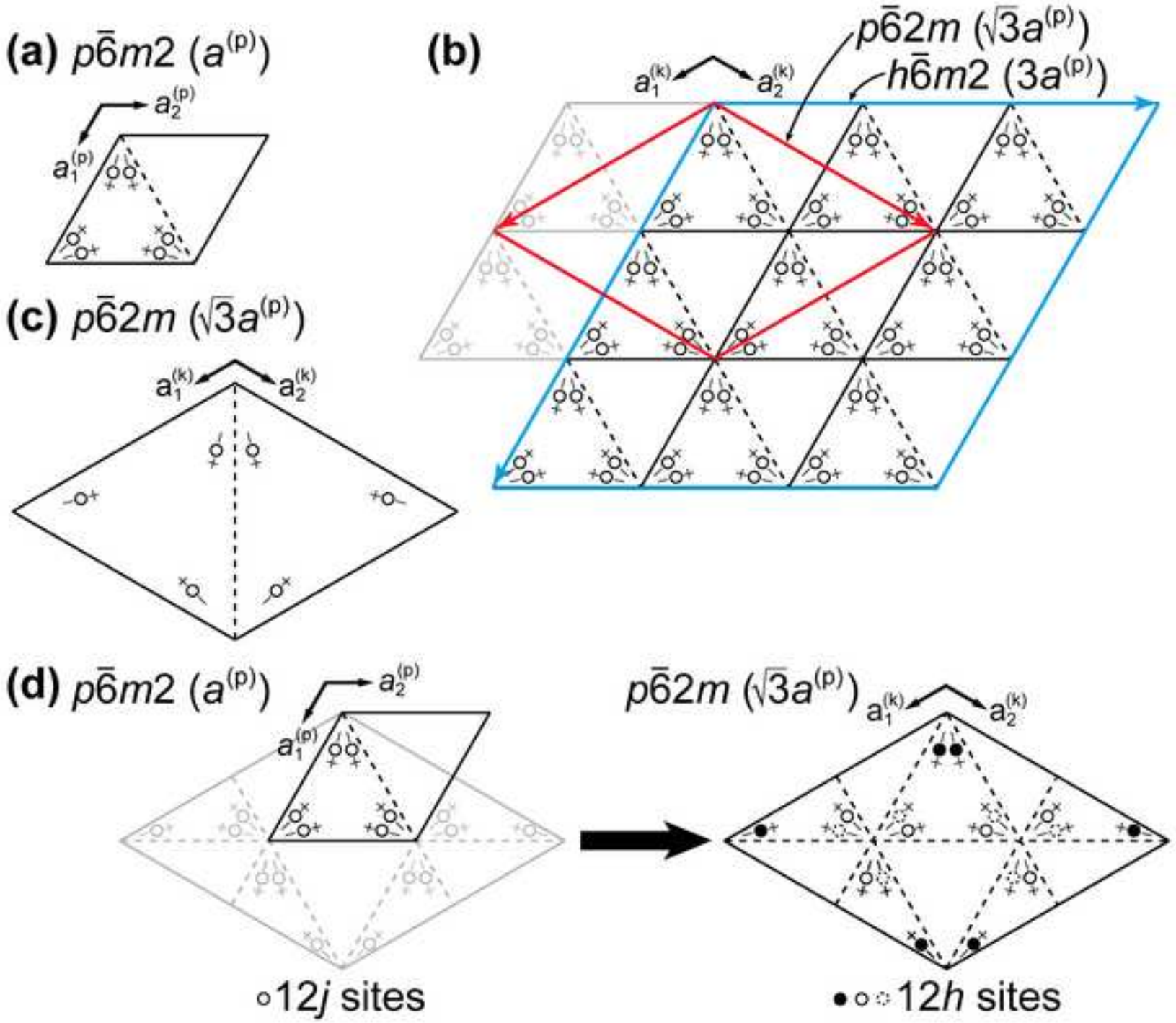

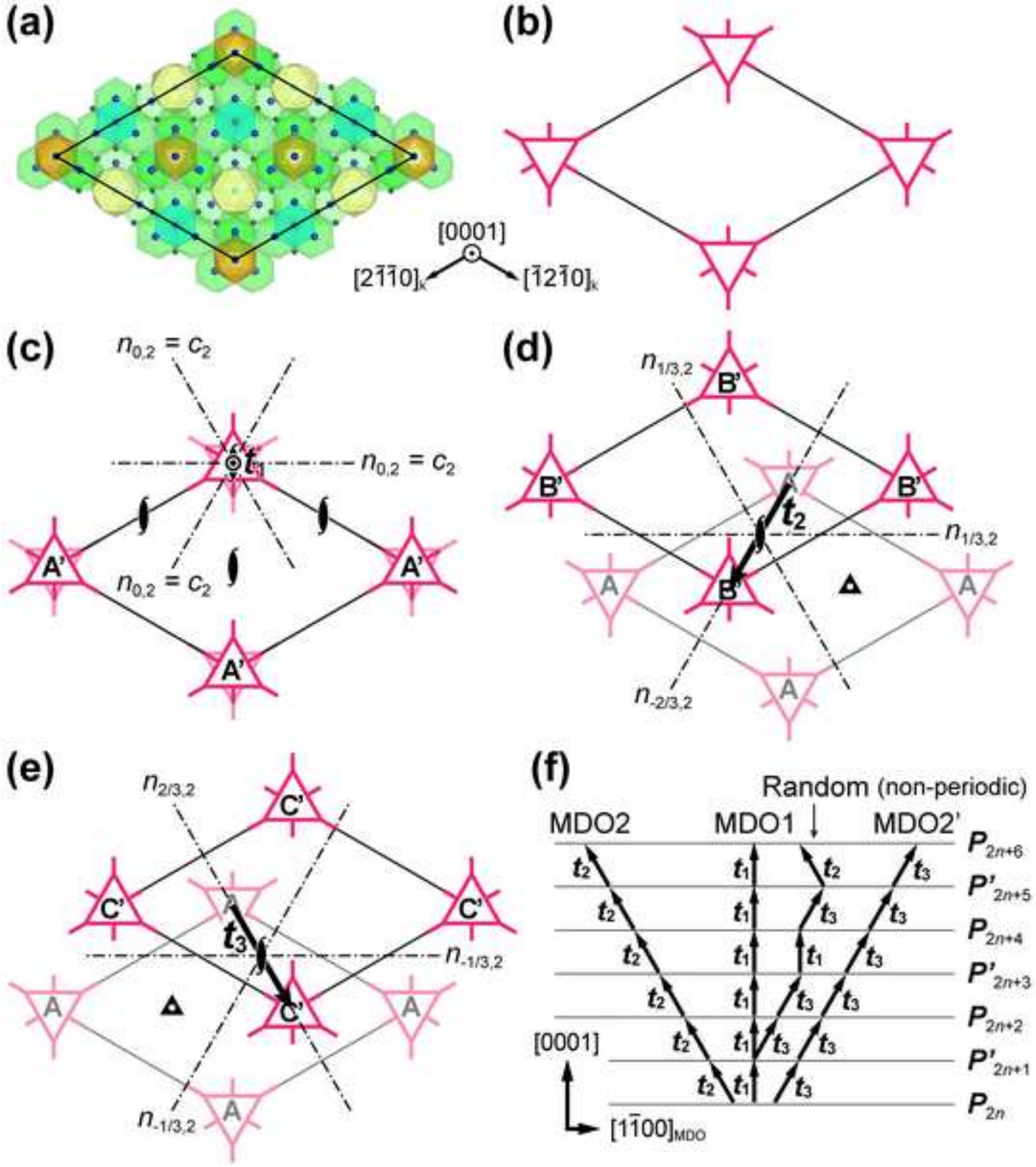

Figure8

Click here to download high resolution image

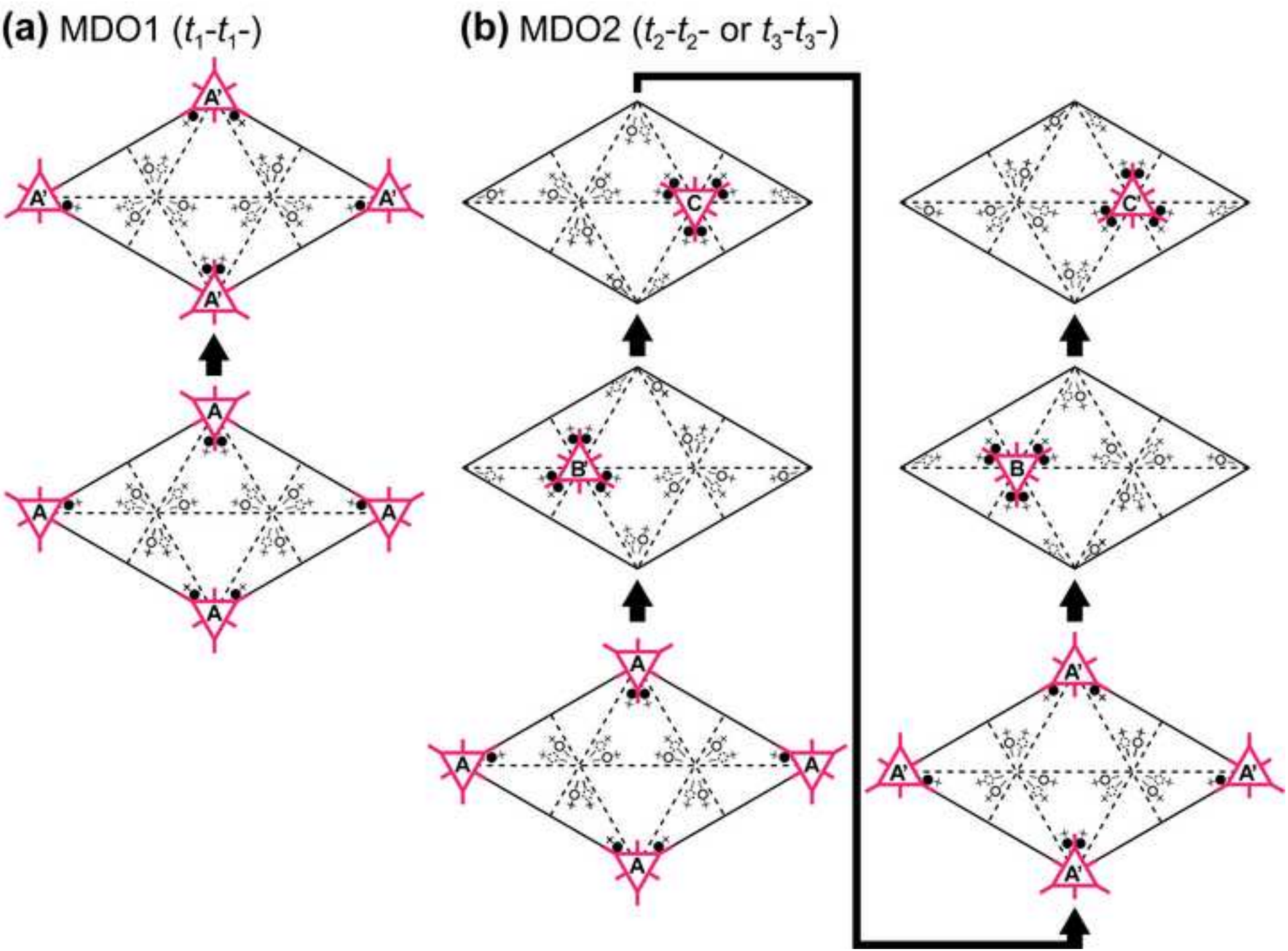

Figure9

Click here to download high resolution image

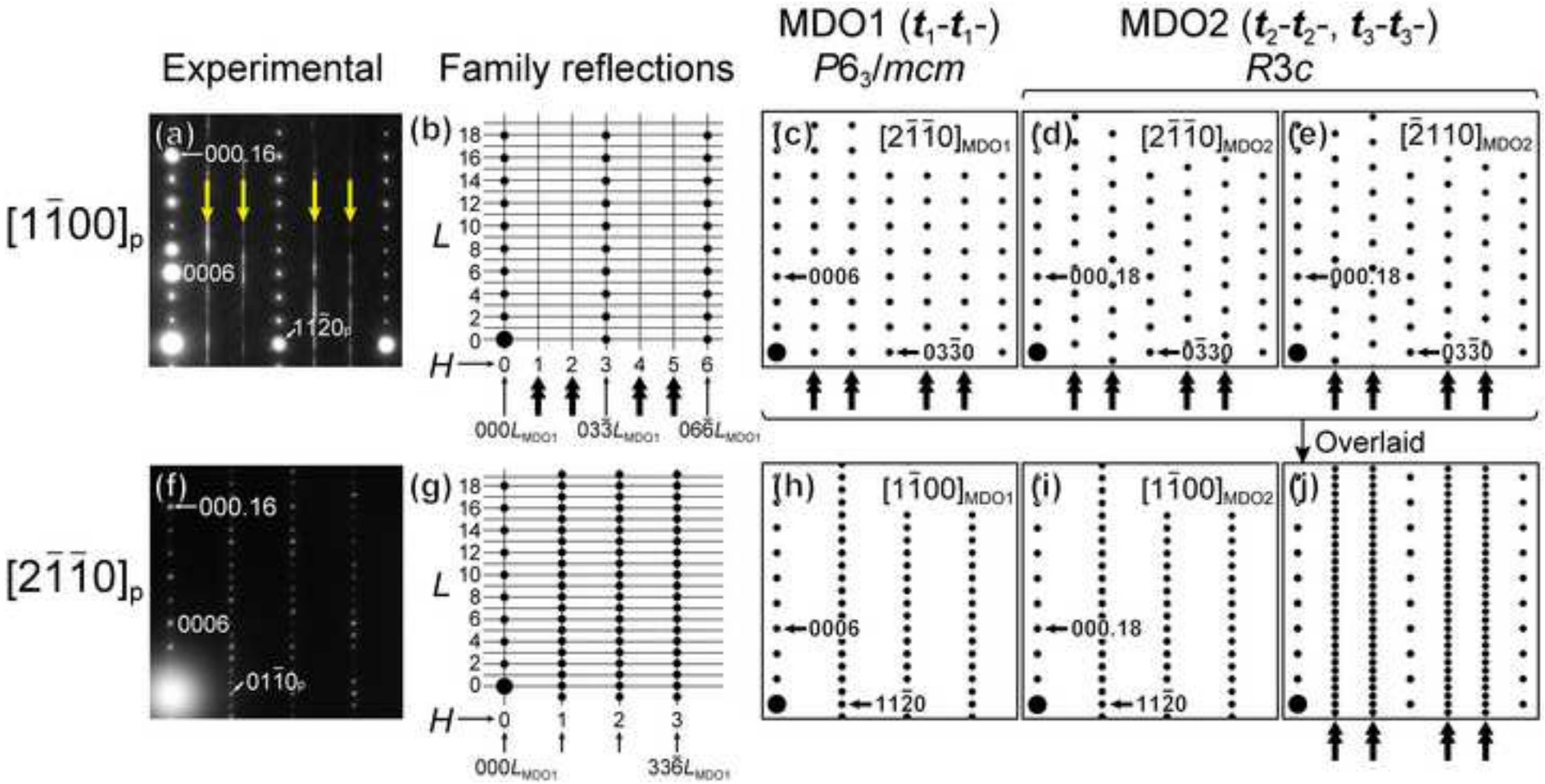

Figure10

Click here to download high resolution image

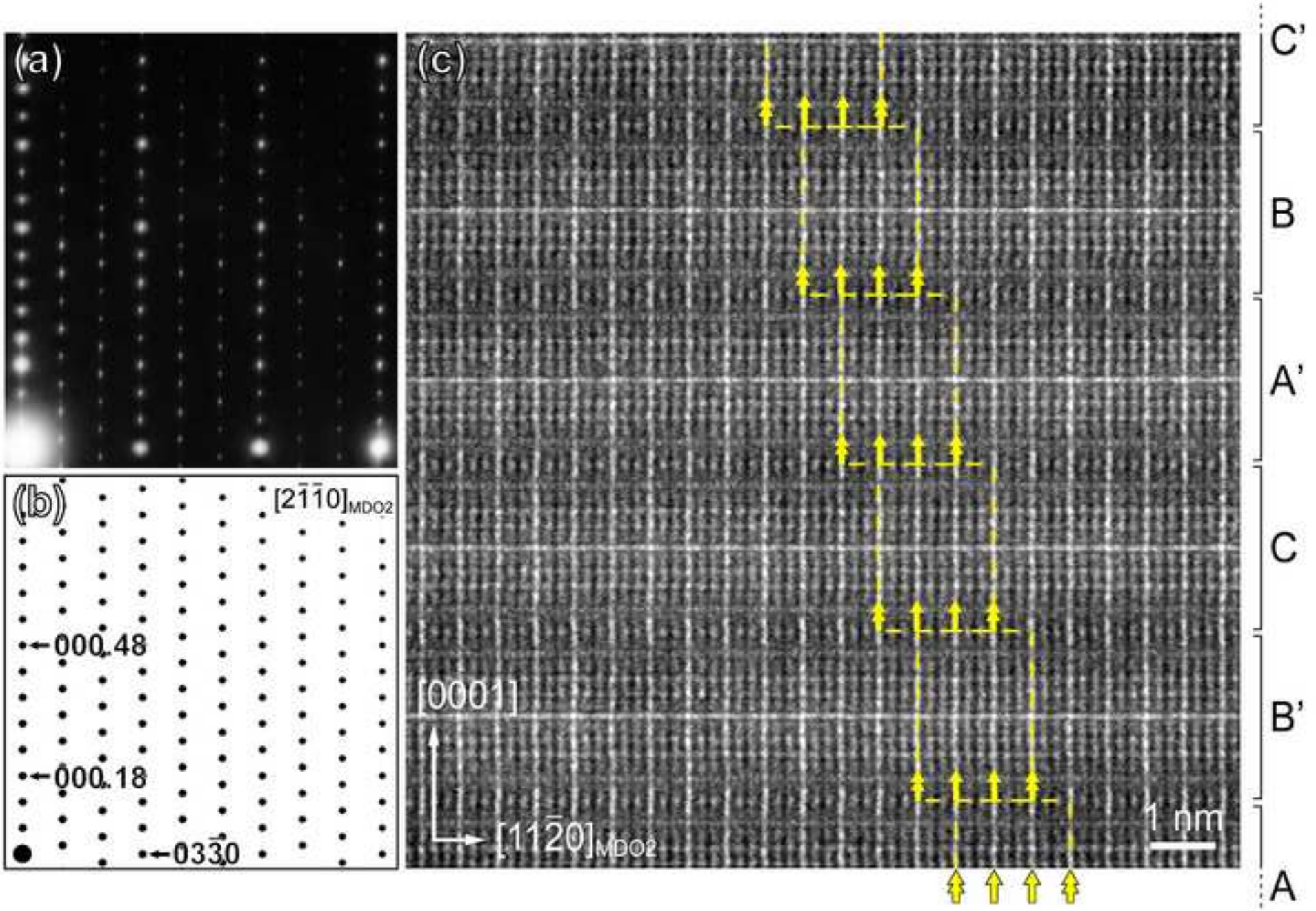

Supplementary Table

Graphical Abstract (for review)